In-Situ Measurement of Interfacial pH Using a Rotating Ring-Disk Electrode

Sholeh Hessami and Charles W. Tobias
Chemical Engineering Dept. and Lawrence Berkeley Laboratory, University of California, Berkeley, CA 94709

A nonintrusive technique for the in-situ measurement of interfacial pH and current efficiency has been developed. A ring electrode, operated potentiometrically at open-circuit, is used to measure the pH change at a rotating disk electrode. The technique takes advantage of the well-characterized hydrodynamics at the rotating disk electrode and has the added advantage that the pH probe, the ring electrode, is not interfering with the flow field and the current distribution on the disk. To determine the pH at the disk electrode by measuring the potential of the ring, the radial transport of hydronium ions across the insulating gap and on the ring is analyzed taking into account the effect of homogeneous dissociation reactions of water and metal-hydroxide ion complexes. Shifts in the ring potential caused by hydrogen super-saturation and ohmic drop are also evaluated. A platinized ring electrode in a hydrogen-saturated electrolyte is shown to provide a stable and reproducible hydrogen ion sensor with a Nernstian response to the changes in the bulk pH. Performance of the ring is evaluated by generating hydrogen at the disk electrode from a dilute acid solution, in the absence of other electrochemical reactions. The technique is then applied to determine the interfacial pH of nickel, iron and nickel-iron alloy electrodeposition with concurrent hydrogen evolution. This method was also used to measure the current efficiency of nickel electrodeposition in a fast, nonintrusive and in-situ manner.

Background

Electrochemical processes such as corrosion, electrosynthesis, and electrodeposition often result in pH changes at the electrode-solution interface. The interfacial pH may differ considerably from that in the bulk solution, and in turn may affect the charge transfer process occurring at the electrode surface. In a review article, Kuhn (1983) affirms the importance of pH measurement near the electrode surface, and discusses various techniques, including colorimetric and optical, sampling, and electrometric methods. The last of these techniques involves placement of a pH sensitive electrode in the vicinity of the working electrode. For example, antimony microelectrodes (Matulis and Slizys, 1964), flat bottomed glass electrodes positioned behind thin, fine mesh cathodes (Romankiw, 1987), and platinized platinum or bismuth embedded in the working electrodes (Gunther et al., 1979) have been used to measure pH at the electrode surface.

Bek and Borodikhina (1978) were first to propose that a rotating disk electrode with a concentric pH sensitive ring could be used for *in-situ* measurement of pH at a disk, but offered neither theory nor experimental results. Using the ring as a pH probe takes advantage of the well-characterized hydrodynamics of the rotating disk electrode without interfering with the flow field and the current distribution on the disk (Figure 1). To date, Albery et al. (1983, 1989) have reported the only actual application of this method for surface pH measurement. Albery and Calvo (1983) used a bismuth-oxide ring electrode in 0.1 M $NaClO_4$ solution with a bulk pH of 7. Generation of H^+ and OH^- on gold, nickel and thionine-modified electrodes were investigated. No measure of the ohmic drop as sensed by the ring was reported; however, the currents passed at the disk were lower than 100 μA which implies that the ohmic component could have been insignificant. Albery and Mount (1989) used the bismuth-oxide ring electrode to measure the flux of protons and hydroxyl ions in and out of a thionine-coated

Present address of S. Hessami: IBM Corporation, 5600 Cottle Rd, San Jose, CA 95193.

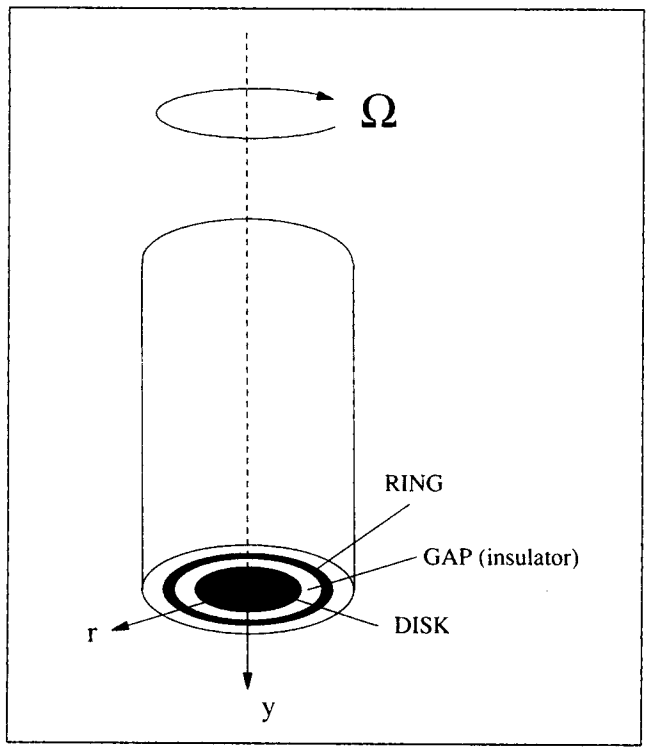

Figure 1. Rotating ring-disk electrode (RRDE).
The ring electrode is kept at open circuit potential.

electrode in solutions with the bulk pH ranging from 4 to 9. The authors concluded that, unlike what was previously thought, electron transfer and not the counter-ion diffusion is the rate limiting-step in the charge transfer process.

In this work, the effect of hydrogen evolution at the disk electrode on the interfacial pH rise and the subsequent ring response, monitored at open circuit, are investigated. We have used a platinum-black ring in hydrogen-saturated solution as the pH sensor. We will focus on the electrodeposition of nickel, iron, and nickel-iron alloy which involve simultaneous hydrogen evolution. As with practical systems, the bulk pH is kept above 2 to obtain a reasonable current efficiency, and below 4 to avoid precipitation of metal-hydroxide solids, $M(OH)_2$. Measurement of the interfacial pH is important in understanding the mechanism of electrodeposition of these metals. In particular, it is known that during electroplating of the iron group alloys, the rate of deposition of the noble component (that is, thermodynamically more favored for reduction) is inhibited in the presence of the less noble component. For example, iron suppresses nickel deposition during nickel-iron alloy electrodeposition. Among various proposed hypotheses for this so called "anomalous codeposition" of nickel-iron, a mechanism involving ferrous hydroxide blocking the discharge of nickel is well known (Dahms and Croll, 1965). For the formation of a hydroxide film of nickel or iron, the required interfacial pH is higher than 6.5 (Pourbaix, 1974). We have used the Rotating Ring Disk Electrode System (RRDE) technique to monitor the interfacial pH rise caused by hydrogen evolution during nickel, iron and nickel-iron alloy electrodeposition. In the case of nickel, we have used the RRDE method to also determine the current efficiency of electrodeposition.

The current densities for electrodeposition in the present study range from 1-20 mA/cm^2, considerably higher than the current densities in the systems studied by Albery et al. At these current densities the ohmic component of the ring response can significantly affect the accuracy of the measurement and must be evaluated. Moreover, the effects of metal-hydroxide ions which can strongly buffer the pH rise, and that of hydrogen gas super-saturation on the ring potential must be considered.

Theory

Transport in the RRDE

In comparison to placing an ion-selective electrode such as a pH sensor in the axial direction, positioning the sensor radially on the plane of the electrode offers a higher degree of sensitivity. This point can be better understood if the concentration variations in the radial and axial directions are compared. Consider the convective diffusive transport of a single reacting species in the presence of supporting electrolyte. The thinness of the diffusion layer (high Sc number) and a large Peclet number in the radial direction allows simplification of the material balance to the following form:

$$ay\Omega\left(\frac{\Omega}{\nu}\right)^{1/2}\left(r\frac{\partial C}{\partial r}-y\frac{\partial C}{\partial y}\right)=D\frac{\partial^2 C}{\partial y^2} \tag{1}$$

where migration is assumed negligible, and there are no homogeneous chemical reactions. The disk electrode is taken to be uniformly accessible to the electro-active species, an assumption which holds strictly at limiting current. Far away from the electrode, the concentration approaches that of the bulk solution. The normalized concentration profile, Θ, in the disk zone, known as the Levich equation is:

$$\Theta=\frac{C-C^d}{C^b-C^d}=\frac{1}{\Gamma(4/3)}\int_0^{\zeta}e^{-x^3}dx \tag{2}$$

where $\zeta=y(\Omega/\nu)^{1/2}(a\nu/3D)^{1/3}$ is the dimensionless axial distance from the electrode.

Depletion of the electro-active species, caused by the disk reaction, is sensed downstream by the ring electrode. In the open-circuit, potentiometric application of the RRDE, the normal flux of the electro-active species to the ring is zero since no net charge-transfer reaction occurs. Therefore, the ring can also be considered as part of the gap or insulator region. Albery and Brukenstein (1966) have carried out the solution to this problem in the gap and ring regions by using the Laplace transformation of the r variable. Smyrl and Newman (1972) applied the Lighthill transformation and superposition integrals to solve the above problem. Both methods lead to the following description of the radial concentration profile on the plane of the electrode beyond the disk surface:

$$\Theta_{(r,\ y=0)}=\frac{C_{(r)}-C^d}{C^b-C^d}=F(\rho) \tag{3}$$

where

$$\rho=\left(\frac{r}{r_0}\right)^3-1$$

and

$$F(\rho)=\frac{1}{4}+\frac{3}{2\pi}\tan^{-1}\left[\frac{2\rho^{1/3}-1}{\sqrt{3}}\right]+\frac{\sqrt{3}}{4\pi}\ln\left[\frac{(1+\rho^{1/3})^3}{1+\rho}\right] \quad (4)$$

Equation 3 relates the concentration at the disk surface, C^d, to the concentration at other points on the plane of the RRDE, $C_{(r)}$. This relationship depends only on the geometry: the disk radius, r_0, and the radial distance from the center of the disk.

In Figure 2 a map of normalized concentration away from the disk electrode, both in the axial direction, and radially on the plane of RRDE, is shown. It can be seen that for a rotation speed of 900 rpm, $D_i=10^{-5}$ cm^2/s, $\nu=0.01$ cm^2/s, and $r_0=0.4$ cm, the axial variation in concentration occurs over the mass-transfer boundary layer thickness of 20 μm. In the radial direction, the variation in concentration takes place over much larger distances. As an example, for detecting $\Theta=0.5$, the probe could be placed 7 μm away from the disk surface axially, or 300 μm away from the edge of the disk, on the plane of RRDE. In other words, while in the axial direction mass-transfer limitations are confined to a very small region, in the radial direction convection carries the depleted solution to much larger distances. This implies that the ring electrode as a probe is not only nonintrusive, but should also have a very good sensitivity for detecting concentration changes.

Interfacial pH rise at the disk caused by hydrogen evolution

When base metals such as iron, nickel, and cobalt are electroplated, hydrogen evolution takes place simultaneously. In aqueous media, the transport of protons is coupled with other species such as hydroxyl ions, metal-hydroxide complexes, and buffers. The presence of other electro-active species such as discharging metal ions during electroplating, requires modification of the analysis presented in the previous section for a single reactive species. For metal deposition and hydrogen reduction, the electrode reactions are:

$$H^+ + e^- \rightarrow \frac{1}{2}H_2$$

$$H_2O + e^- \rightarrow \frac{1}{2}H_2 + OH^-$$

$$M^{+2} + 2e^- \rightarrow M$$

$$MOH^+ + 2e^- \rightarrow M + OH^-$$

$$M^{+2} + H_2O + e^- \rightarrow \frac{1}{2}H_2 + MOH^+$$

The concentration of hydrogen and hydroxyl ions are coupled through the water dissociation equilibrium maintained throughout the solution:

$$C_{H^+}C_{OH^-}=K_w \quad (5)$$

Metal-hydroxide ions, MOH^+, which are formed by hydrolysis (Sillen, 1959) buffer the pH rise caused by hydrogen evolution:

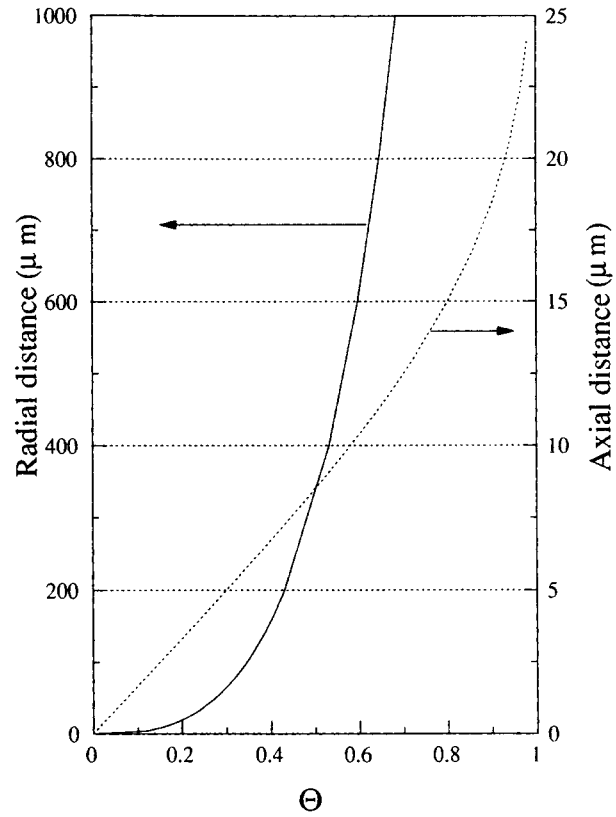

Figure 2. Comparison of radial and axial variation of normalized concentration, 900 rpm, disk radius = 0.4 cm.

$$M^{+2} + H_2O \leftrightarrows MOH^+ + H^+$$

Taking into account the homogeneous reactions of metal-hydroxide ions and water dissociation, the material balance for hydrogen ions becomes:

$$\nabla\cdot N_{H^+} - \nabla\cdot N_{OH^-} - \nabla\cdot_{MOH^+} = 0 \quad (6)$$

If formation of bubbles and surface films such as metal-hydroxide precipitates can be neglected, the convective-diffusive material balance of Eq. 6 can be rewritten as:

$$a y \Omega \left(\frac{\Omega}{\nu}\right)^{1/2} \times \left[r\frac{\partial(C_{H^+}-C_{OH^-}-C_{MOH^+})}{\partial r} - y\frac{\partial(C_{H^+}-C_{OH^-}-C_{MOH^+})}{\partial y}\right] = D_{H^+}\frac{\partial^2}{\partial y^2}\left[C_{H^+} - \frac{D_{OH^-}}{D_{H^+}}C_{OH^-} - \frac{D_{MOH^+}}{D_{H^+}}C_{MOH^+}\right] \quad (7)$$

The boundary condition at the disk is related to the hydrogen current:

$$\frac{i_{H_2}}{F} = -D_{H^+}\frac{\partial}{\partial y}\left[C_{H^+} - \frac{D_{OH^-}}{D_{H^+}}C_{OH^-} - \frac{D_{MOH^+}}{D_{H^+}}C_{MOH^+}\right]_{y=0} \quad (8)$$

The exact solution to this full two dimensional nonlinear

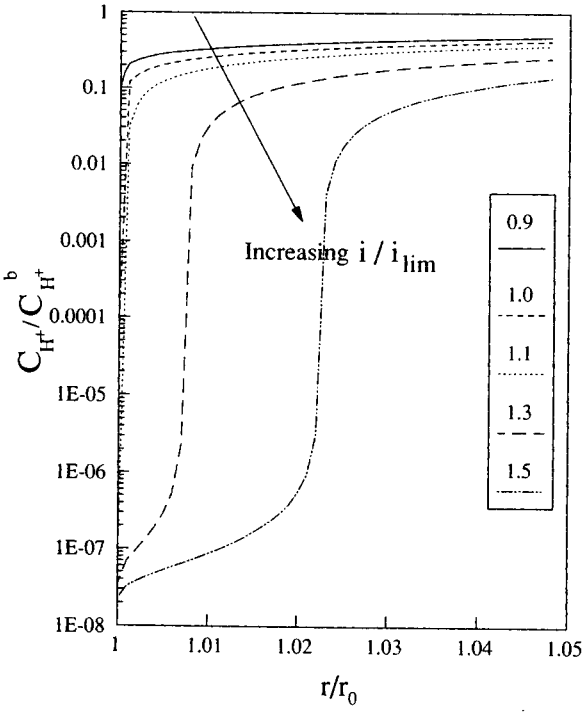

Figure 3. Calculated radial concentration of protons for different fractions of hydrogen limiting current, bulk pH = 3.

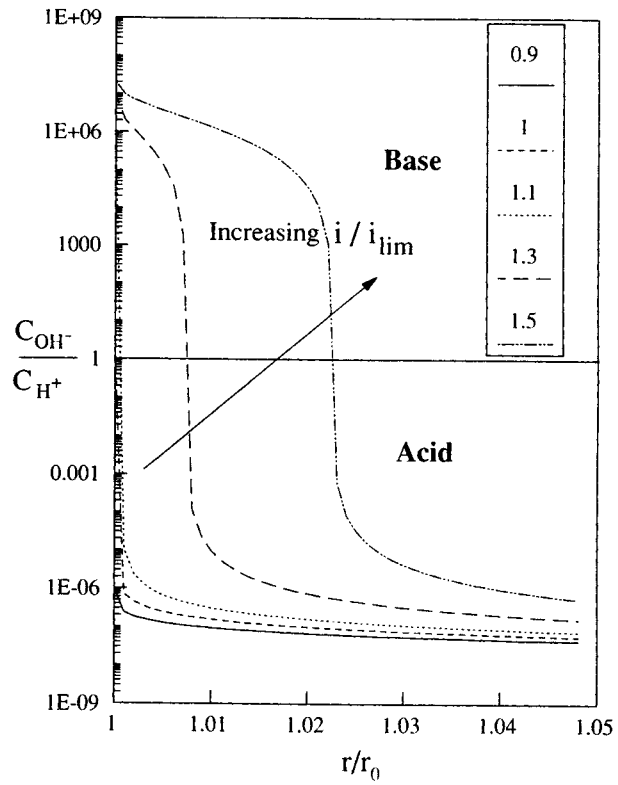

Figure 4. Calculated acid-base transition on the plane of the RRDE, bulk pH = 3.

problem requires a numerical method. However, the analytical results obtained by superposition integrals can be used if the problem is linearized by the approximation of equal diffusivities. Qualitatively, the equal diffusivity approximation assigns a higher diffusion coefficient to the hydroxyl containing ions which means that the concentration of these species at the disk surface and downstream in the radial direction is underestimated.

The equal-diffusivity approximation simplifies Eqs. 7-8 to the following form:

$$ay\Omega\left(\frac{\Omega}{\nu}\right)^{1/2}\left(r\frac{\partial\overline{C}}{\partial r}-y\frac{\partial\overline{C}}{\partial y}\right)=D\frac{\partial^2\overline{C}}{\partial y^2} \tag{9}$$

$$\frac{i}{F}=-D\left.\frac{\partial\overline{C}}{\partial y}\right|_{y=0} \tag{10}$$

where

$$\overline{C}=C_{H^+}-C_{OH^-}-C_{MOH^+} \tag{11}$$

Similar to Eq. 3, the concentration varies radially as described by:

$$\frac{\overline{C}_{(r)}-\overline{C}^b}{\overline{C}^d-\overline{C}^b}=1-F(\rho) \tag{12}$$

and $\overline{C}^d$ can be related to the current density of hydrogen evolution at the disk electrode:

$$I=\frac{i}{i_{\text{lim, }H^+}}=\frac{\overline{C}^b-\overline{C}^d}{C_{H^+}^b} \tag{13}$$

where $i_{\text{lim, }H^+}$ is the hydrogen-ion limiting current in the absence of MOH^+ ions. Rearranging Eq. 12 and using Eq. 13 gives:

$$\frac{\overline{C}_{(r)}}{\overline{C}^b}=1-I\frac{C_{H^+}^b}{\overline{C}^b}(1-F) \tag{14}$$

With the above general formulation, it is useful to consider the base case of hydrogen evolution in the absence of metal deposition. For various fractions of the hydrogen-ion limiting current, the radial variation of C_{H^+} normalized to $C_{H^+}^b$ is shown in Figure 3. Unless otherwise stated, the bulk pH is taken to be equal to 3.0 in the calculations. At current densities exceeding the limiting current, the solution near the plane of the RRDE becomes alkaline. The transition from basic to acidic regions, extending to the gap and ring regions, is shown in Figure 4. Depending on the size of the disk electrode, pH rise can occur over large radial distances. If the ring material responds to the activity of protons reversibly, that is, following the Nernst equation, for every decade decrease in concentration a -59.1 mV shift in the ring potential will be observed at 25°C:

$$E=E^0+\frac{RT}{F}\ln\frac{a_{H^+}}{P_{H_2}^{1/2}}=0+59.1\log\frac{a_{H^+}}{P_{H_2}^{1/2}} \tag{15}$$

The ring potential is a radial average because of its finite thickness. Using an Extended Trapezoidal Rule (for example,

Table 1. Dimensions of the Ring-Disk Geometries

Geometry	r_0(cm)	r_1(cm)	r_2(cm)
A	0.383	0.398	0.422
B	0.383	0.416	0.557

Press et al.), we have numerically calculated the radial average of proton concentration for two different RRDE geometries listed in Table 1. The resulting shift in the ring potential vs. fraction of the hydrogen limiting current passed at the disk is shown in Figure 5. It should be noted that the interfacial pH rise and the associated cathodic shift in the ring potential depend on the fraction of the hydrogen ion limiting current, and not on the magnitude of the hydrogen current. In other words, for a constant hydrogen current, the fraction of the limiting current depends on the bulk pH and agitation rate.

The buffering effect of MOH^+ ions

In the presence of metal-hydroxide ions, the pH rise is buffered. If we assume that the homogeneous reactions are much faster than the transport processes, the concentration of MOH^+ ions can be related to those of protons and metal ions by an equilibrium relationship:

$$C_{MOH^+} = \frac{K_w C_{M^{+2}}}{K_d C_{H^+}} \tag{16}$$

where K_d is the dissociation constant for MOH^+ ions.

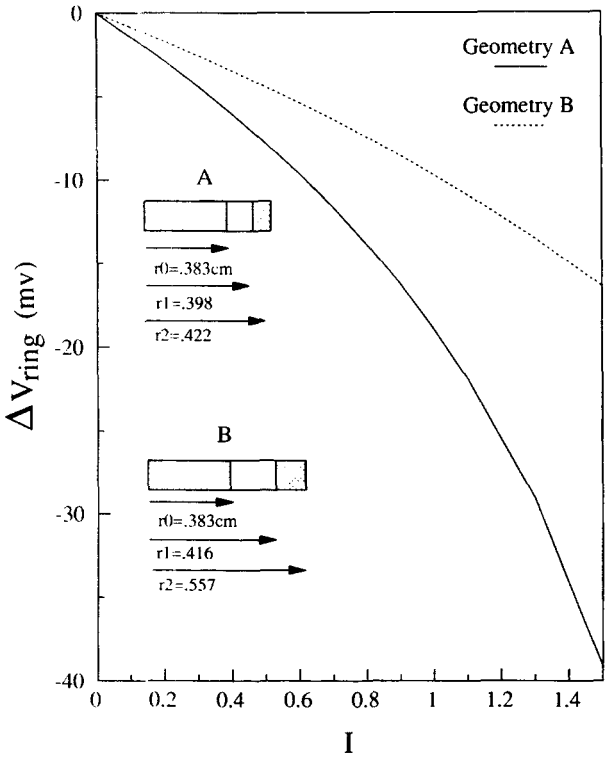

Figure 5. Predicted ring response to the fraction of hydrogen ion limiting current.

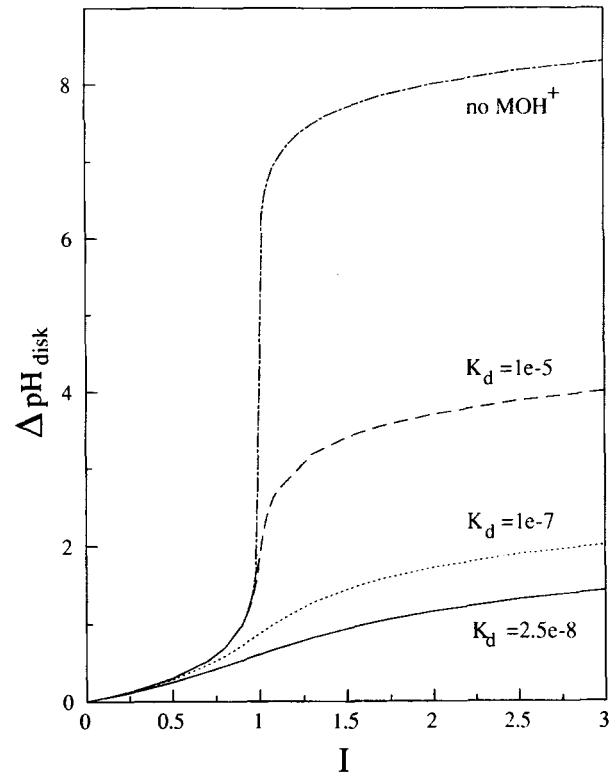

Figure 6. Calculated interfacial pH rise at the disk vs. fraction of hydrogen limiting current, bulk pH = 3, 0.2 M metal ions.

The dissociation equilibrium of MOH^+ ions cushions the buildup of hydroxide ions, resulting in a higher hydrogen ion concentration compared to the case where no metal-hydroxide ions are present. Thus, the pH rise caused by hydrogen evolution is reduced both at the electrode surface and throughout the solution. The reduction of the disk interfacial pH rise in the presence of metal-hydroxide ions is demonstrated in Figure 6. The values for the dissociation constants are typical for metal-hydroxide ions of base metals. As seen in Figure 6 the buffering effect of MOH^+ becomes more pronounced with decreasing K_d value. Note that, for example, $I = 1.5$ means the current going into hydrogen evolution is 1.5 times the hydrogen limiting current in the absence of MOH^+ ions. Here the total concentration for metal ions C_{TM} is 0.2 M, and it is assumed that this concentration remains constant throughout the solution. This is only an approximation because if a significant fraction of the limiting current for metal deposition passes through the disk electrode, depletion of the metal ions becomes important. Under this assumption, the relationship between the C_{MOH^+} and proton concentration can be expressed as:

$$C_{MOH^+} = \frac{C_{TM}}{1 + \frac{K_d}{K_w} C_{H^+}} \tag{17}$$

Suppression of pH rise in the presence of metal-hydroxide ions is related to the enhancement of hydrogen ion limiting current by metal-hydroxide ions:

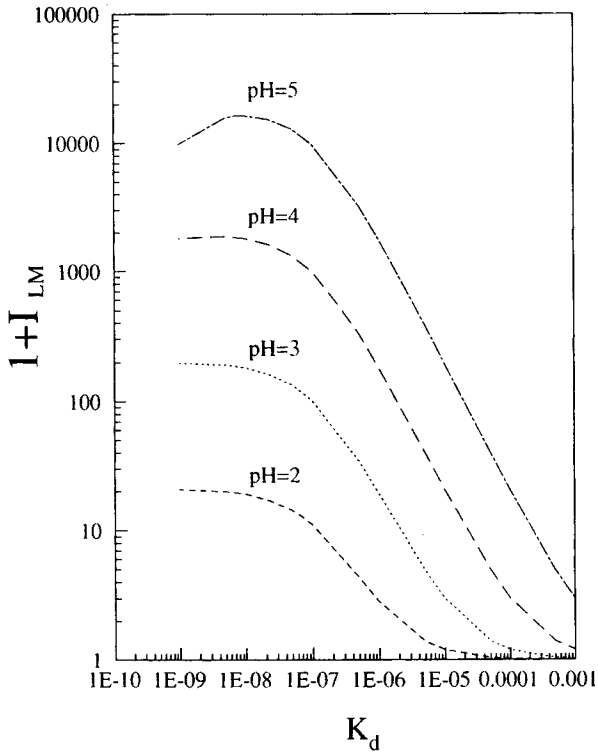

Figure 7. Enhancement of hydrogen limiting current in the presence of 0.2 M metal ions.

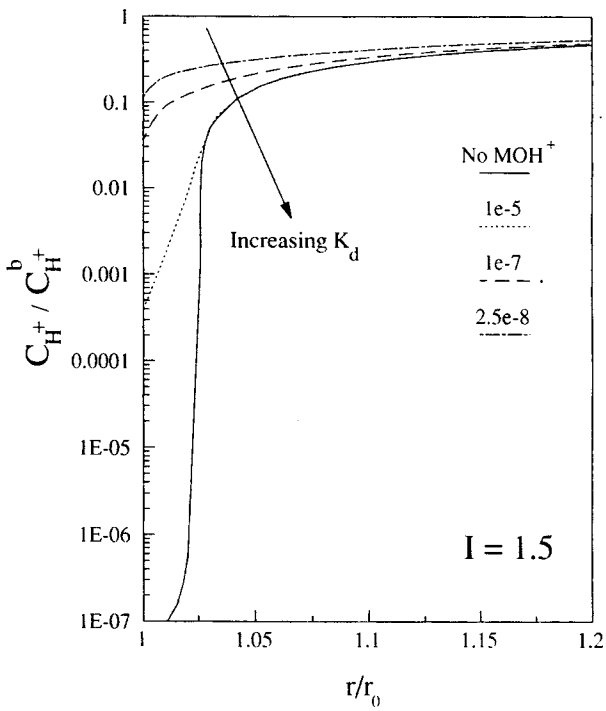

Figure 8. Effect of metal-hydroxide ions on the radial concentration of protons.

$$\frac{i_{\text{lim}}}{i_{\text{H}^+,\text{lim}}} = 1 + I_{LM} = 1 + \frac{C^d_{\text{MOH}^+} - C^b_{\text{MOH}^+}}{C^b_{\text{H}^+}} \tag{18}$$

Shown in Figure 7 is the dependence of I_{LM} on K_d for various bulk pH values. The smaller the dissociation constant of metal-hydroxide ions, K_d, the larger the enhancement of the limiting current becomes. The maximum obtainable enhancement depends on the bulk pH and MOH^+ concentration. For example, at pH = 2 and 0.2 M total metal ion concentration, the maximum I_{LM} is 20. The practical implication of these results is that for a given bulk pH and agitation rate a substantially higher hydrogen current can be passed at the disk electrode before the interfacial pH becomes high enough to allow the precipitation of metal-hydroxide solids, $M(OH)_2$.

An example of the radial profile of hydrogen ions in the presence of MOH^+ is shown in Figure 8. These values were calculated by solving a quadratic equation resulting from Eqs. 11, 14 and 17 at $I = 1.5$. The radial average over the finite thickness of the ring is related to the interfacial pH rise at the disk electrode.

Effect of H_2 supersaturation on the ring potential

A reversible ring to hydrogen evolution reaction responds to the changes in both pH and hydrogen pressure. With hydrogen gas evolution at the disk electrode, there will be some supersaturation which is sensed by the ring with a corresponding shift in the potential, described by the Nernst equation, Eq. 15. The increase in the dissolved hydrogen concentration at the disk electrode can be related to the current density as follows:

$$\frac{C^d_{\text{H}_2}}{C^b_{\text{H}_2}} = 1 + \frac{1}{2}\frac{C^b_{\text{H}^+}}{C^b_{\text{H}_2}}\frac{i}{i_{\text{lim,H}^+}} \tag{19}$$

where it was assumed that the diffusivities of dissolved hydrogen and protons are the same. This is not a bad assumption since available experimental data (for example, Shibata, 1960, or Perry and Chilton, 1973) indicate a diffusion coefficient of 1×10^{-5} cm^2/s for hydrogen in aqueous electrolytes.

The bulk concentration of H_2 can be approximated from Henry's Law constant. Prausnitz et al. (1986) report for the solubility of the H_2 in pure water

$$\log\left(\frac{f}{x}\right) = 4.86 = \log H_{\text{H}_2} \tag{20}$$

which means that for 1 atm hydrogen gas pressure, the mole fraction in water is 1.4×10^{-5}. This translates to a hydrogen solubility of 7.6×10^{-4} M at room temperature, in good agreement with values reported by other workers (see, for example, Ruetschi and Amile, 1966). The hydrogen solubility in electrolyte is lower than that in pure water. This "salting-out" effect is often expressed as:

$$\log \frac{S^0_i}{S_i} = k_s C_s \tag{21}$$

where S_i is the solubility in electrolyte, k_s is the salting-out parameter, and C_s is the salt concentration. Since k_s is a salt specific parameter, we use $k_s = 0.11$ M^{-1} corresponding to NaCl which is the supporting electrolyte in our solutions. In 1.5 M

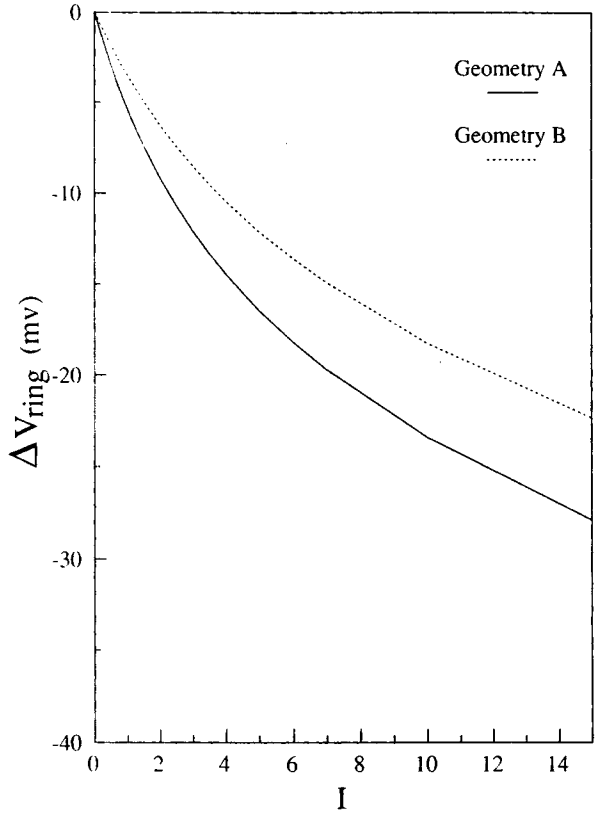

Figure 9. Predicted ring cathodic shift caused by hydrogen super-saturation.

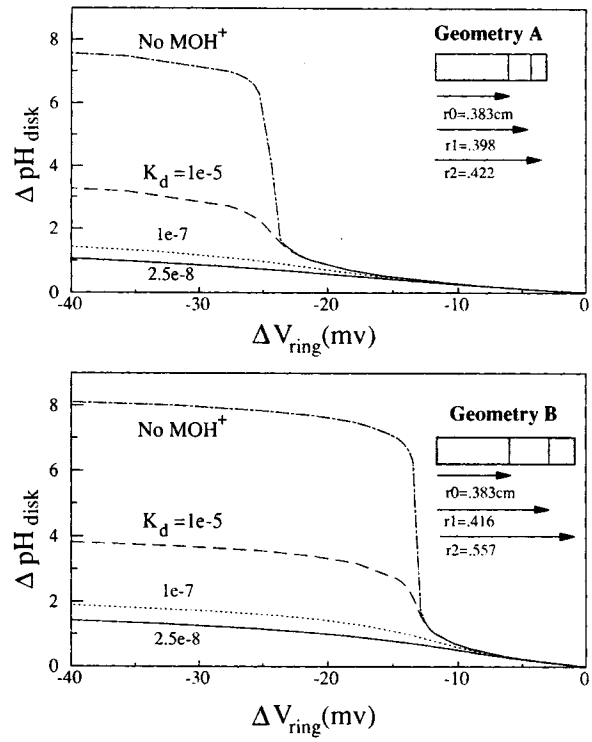

Figure 10. Overall ring response to the disk pH rise in the presence of MOH^+ ions.

NaCl solution, the hydrogen solubility, or the concentration of the dissolved hydrogen, is 5×10^{-4} M. Using this value for $C^b_{H_2}$, and calculating $C^d_{H_2}$ from Eq. 19, we can estimate the radial profile of dissolved H_2 and the cathodic shift in the ring potential, plotted in Figure 9, associated with the hydrogen supersaturation.

The ring response to the changes in the dissolved hydrogen gas concentration is smaller than the shift of potential corresponding to hydrogen ions, as reflected by the difference between the scale of x axis in Figures 5 and 9. This difference can be understood by the stoichiometry of H_2 and H^+ in the hydrogen evolution reaction, and the Nernst slope of -30 mV for each decade increase in the partial pressure of hydrogen (see Eq. 15).

Overall ring response to the interfacial pH rise

The correspondence between the interfacial pH rise at the disk and the ring potential shift is shown in Figure 10 for various values of metal-hydroxide dissociation constants, K_d, and two geometries. The ring response includes the combined contributions of hydrogen ion depletion, buffering effect of metal-hydroxide ions, and supersaturation of dissolved hydrogen. The calculation is based on a bulk pH of 3, dissolved hydrogen gas concentration of 5×10^{-4} M and 0.2 M metal ions. The interfacial pH rise is significantly reduced by the buffering action of metal-hydroxide ions. In the absence of metal-hydroxide ions, or for large values of K_d, there is a threshold in the ring potential shift which corresponds to a titration at the disk when the hydrogen limiting current is exceeded. The hydroxyl ions generated are used up in the homogeneous reaction of MOH^+ formation leading to the marked decrease in the disk interfacial pH rise. As seen in Figure 10, the threshold potential shift is -22 mV for geometry A and -12 mV for geometry B. For cathodic shifts smaller than the threshold values, the interfacial pH rise is less than two units, while for larger ring responses, the pH rise varies significantly depending on the dissociation constant of metal-hydroxide ions present. It is interesting to note that in the presence of metal-hydroxide ions, a given shift in the ring potential not only corresponds to a lower interfacial pH rise, but also a higher hydrogen current.

Ohmic component

Although no current is passed through the ring electrode, it registers an ohmic potential drop because passage of current through the electrolyte establishes an electric field. The potential distribution for our application of the RRDE is closer to the case of uniform current distribution on the disk, or that of mixed kinetics and mass-transfer control in the case of simultaneous hydrogen and metal deposition. However, the well-known primary current distribution provides an upper bound for the potential distribution outside the disk region. (Primary current distribution assumes that the potential obeys Laplace's equation everywhere and there is no resistance to charge transfer at the electrode surface.) It is also known that experimental techniques, such as current interrupt, measure the ohmic resistance corresponding to the primary current distribution (Newman, 1970).

The finite thickness of the ring requires calculating the av-

erage potential value. Miksis and Newman (1976) have calculated primary resistances for various ring-disk geometries by superposition. The ohmic resistance between the ring and the disk, R_{rd} was expressed as:

$$\frac{\Phi}{\Phi_0} = \kappa r_2 R_{rd} \frac{4r_0}{r_2}; \qquad \Phi_0 = \frac{I_{tot}}{4\kappa r_0} \tag{22}$$

where Φ_0 is the potential at the disk electrode and the potential Φ is taken to be zero at infinity. The authors have tabulated the values for $\kappa r_2 R_{rd}$. As an example, $r_0/r_1 = 0.9$ and $r_1/r_2 = 0.8$, yields $\Phi/\Phi_0 = 0.588$.

The ohmic drop at the ring is particularly important for metal deposition where high currents are passed. By increasing the conductivity of the electrolyte and by using a smaller disk electrode the ohmic potential drop can be reduced. The insulator thickness is also a key parameter in determining the ohmic drop sensed by the ring. Although the sensitivity of the ring to the changes in pH at the disk surface increases, placing the ring very close to the disk has the disadvantage of being in a region where variations in Φ_0 are very sharp, as seen in Figure 11. The uncertainty in the ohmic component of the ring response can be detrimental to the accuracy of the RRDE method for *in situ* pH measurement.

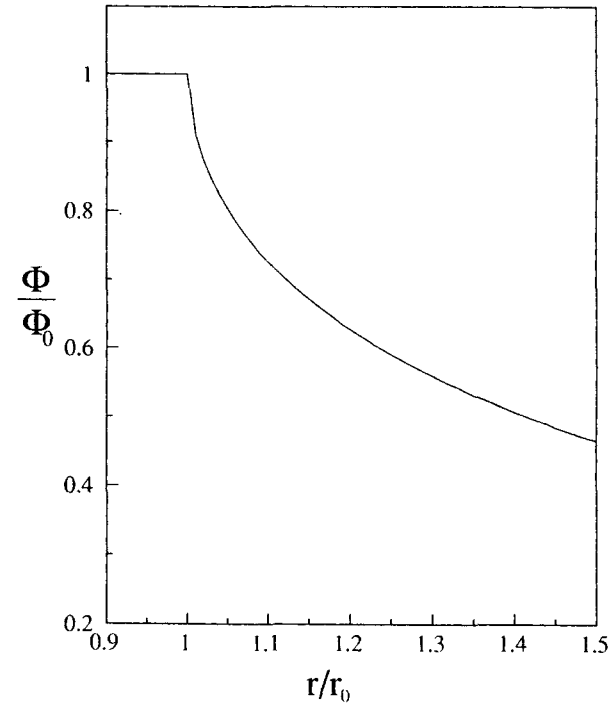

Figure 11. Potential variation on the plane of RRDE calculated from primary current distribution.

Experiments

Experimental apparatus

A platinum-platinum ring-disk electrode made by Pine Instruments Company is employed for all of the RRDE measurements. The dimensions of the RRDE are $2r_0 = 0.765$ cm, $2r_1 = 0.833$ cm, and $2r_2 = 1.113$ cm corresponding to Geometry B. When a different substrate such as nickel is needed for the disk electrochemical reaction, a thin layer of the desired material is electroplated on top of the Pt disk. The potentiometric ring operation as a pH sensor requires a material which is reversible to hydrogen ions. Platinum black is an excellent material for the hydrogen electrode (Hills and Ives, 1961), and can be prepared easily.

A Pine Instruments rotator, model ASRP2, with a speed controller is used to vary the speed of agitation. The counter electrode is a strip of platinum which is housed in one of the glass sections separated from the main cell by a fritted glass. For the measurement of bulk pH a Cole Parmer DigipHase pH meter and a combination glass pH electrode with a calomel reference electrode are employed. Buffer solutions of pH 1.68 and 4.00 (Radiometer Copenhagen) are used for calibration of the pH electrode. A hydrogen atmosphere is maintained before and during experiments by bubbling hydrogen through the solution.

The electrochemical reactions on the disk electrode are controlled by a Potentiostat/Galvanostat Model 273, EG&G Princeton Applied Research. All potential measurements are made against a calomel reference electrode kept in a separate compartment. The current and potential values measured at the disk are displayed on a digital Nicolet 4094 oscilloscope and later transferred to an IBM Personal Systems/2 computer for data analysis and storage. The potential of the ring electrode is monitored at open circuit against the same reference electrode as that of the disk. Since the input impedance of the oscilloscope is not high enough for this purpose, the output of a reference electrode buffer amplifier, AIS-Division of Floyd Bell Associates Inc., model BA-1, is used to display the ring potential on the scope. We found that it was necessary to power the buffer amplifier with batteries to avoid ground loops. This instrumentation allows simultaneous recording of both the ring and the disk potential in addition to the disk current.

The electrolyte conductance is measured by a Wayne Kerr Universal bridge B224 conductivity bridge and a YSI 3401 cell. The cell constant was measured with a 71.1 g/kg solution of KCl at 18°C and found to be 1.22 cm^{-1}.

Experimental procedure

The electrodes are polished following the standard metallographic techniques to a surface finish of 1 μm in roughness. Hellige Certified 1% platinic chloride with 0.012% lead acetate solution is used to deposit platinum black on the ring electrode. High quality deposits with good adherence and electrode coverage are obtained when plated at 2-4 mA/cm^2 with 500 mC of charge passed over the 0.427 cm^2 area of the ring.

All solutions are made with distilled, deionized water. To minimize ohmic effects, that is, to have a better current distribution on the disk and a small ohmic component in the ring pontential shift, 1.0-1.4 M NaCl (certified A.C.S. Fisher Scientific) is used as supporting electrolyte. The bulk pH of electrolyte is adjusted by addition of HCl or NaOH, as needed. The solutions are sparged with H_2 for 10 minutes prior to experiments. Before entering the cell, hydrogen gas (Liquid Carbonic) passes through a sparging column to saturate the gas with electrolyte. The electrodes are dipped in a dilute nitric acid solution and thoroughly rinsed with water before each experiment. The ring potential obtains its equilibrium value

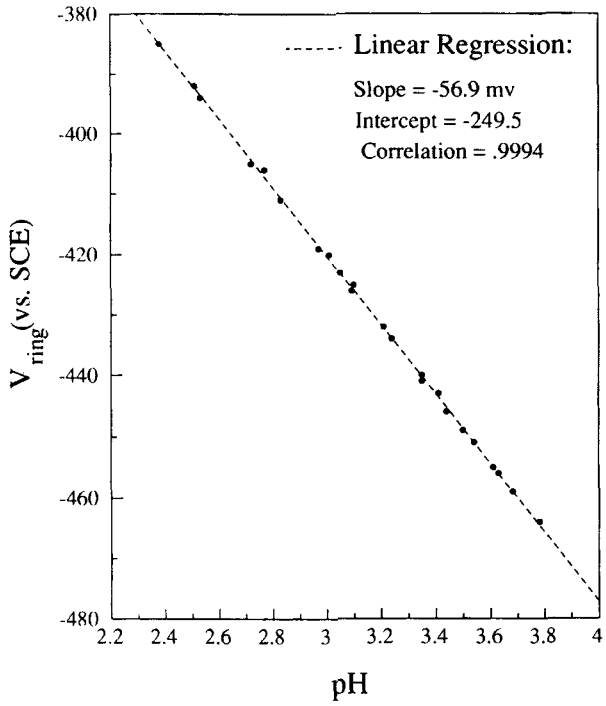

Figure 12. Measured response of the ring to the bulk pH.

very rapidly if the disk is spun to enhance transport of the dissolved hydrogen from the vicinity of the sparger to the bulk.

To insure that the platinized ring electrode in hydrogen atmosphere is working properly, tests were made at various bulk pH values. The ring response to the change in bulk pH is shown in Figure 12 which indicates a slope of 56.9 mV/decade. The theoretical response to hydrogen ion activity is 58.1 mV/decade at 20°C (see Eq. 22). The 1 mV difference between the experiments and theory, equivalent to 0.017 pH units, can be traced back to the uncertainties in the glass pH electrode measuring the bulk pH, buffer solutions used for calibration, and temperature variations. The intercept of the experimental results is -249.5 mV, which is in good agreement with the saturated calomel reference electrode potential on the hydrogen scale: -247.7 mV.

Hydrogen evolution experiments

As the first step for *in-situ* pH measurement at the disk using the RRDE method, hydrogen evolution in the absence of any competing electrochemical reactions was studied. These experiments were considered to be the calibration test of the ring response to the interfacial pH change at the disk. All hydrogen evolution experiments were conducted from dilute acid solutions with 1.4 M NaCl as supporting electrolyte. Steady-state measurements were made by stepping the current at the disk and monitoring the ring potential as shown in Figure 13. Since we are interested in the potential shift of the ring electrode, it is essential that the ring has a stable base line at zero current. This is seen to be the case as shown in Figure 13 where the current is dropped to zero several times and each time the ring potential recovers the same value.

Dynamic experiments were performed by ramping the potential at the disk electrode with simultaneous recording of the disk current and the ring potential. At high current densities, hydrogen bubbles grow which cause some complexities; in addition to altering the current density by covering portions of the disk electrode, radial transport of protons to the ring is hindered by bubbles adhering at the edge of the disk and the inner edge of the ring. The ring response to hydrogen evolution normalized to the proton limiting current, I, as measured by both the steady-state and potential sweep methods is shown in Figure 14. The theoretical cathodic shift in the ring potential is also drawn for comparison. It can be seen that the ring response is suppressed at high currents. The evolved hydrogen has more time to form bubbles during the steady-state measurements compared to the 25 mV/s potential sweep experiments. The complex problem of the effect of bubbles on current distribution has been addressed in the literature (for example, Dukovic et al.) and is beyond the scope of this work.

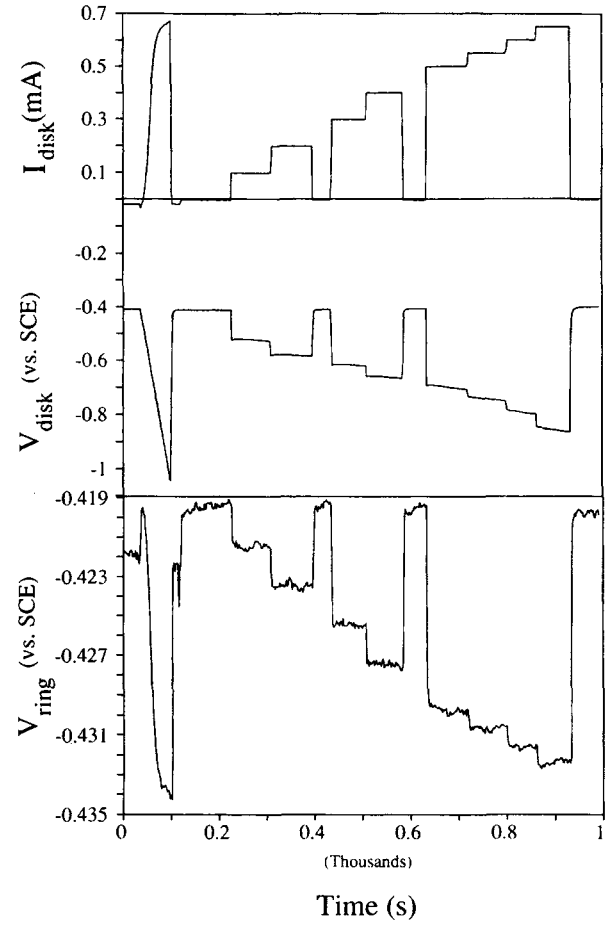

Figure 13. Current-step experiments, hydrogen evolution on platinum from 1.4 M NaCl, pH = 2.95, 900 rpm.

Measurement of the ohmic drop

The current interrupt technique was used to measure the ohmic potential drop registered by the ring. As discussed in the theory section, although the ring is kept at open circuit, it senses the electric field in the solution when current passes through the disk electrode. To obtain the ohmic resistance

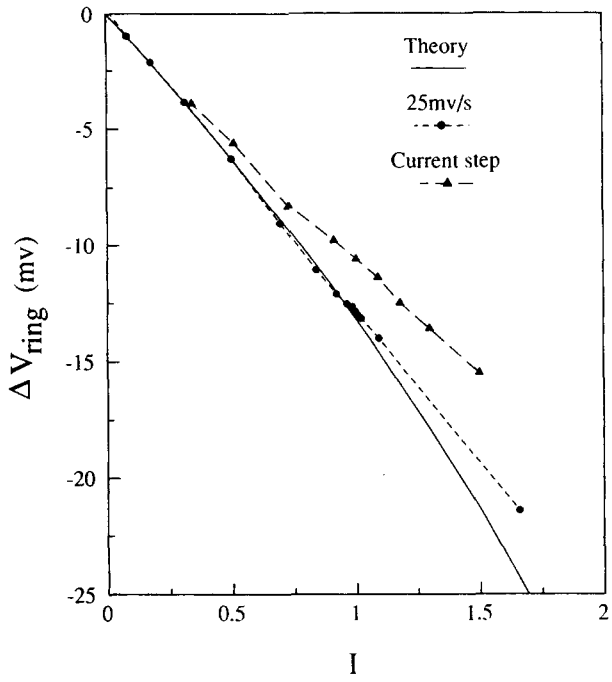

Figure 14. Ring response to hydrogen evolution: current step, potential sweep, and theory.

Suppression of the ring response at high hydrogen currents by adhering bubbles.

between the ring and the reference electrode, the slope of the ohmic potential drop as a function of current should be measured. Figure 15 is an example of one such measurement for a nickel plating solution containing 0.2 M $NiCl_2$, and 1 M NaCl. The slope representing the ohmic resistance between the ring

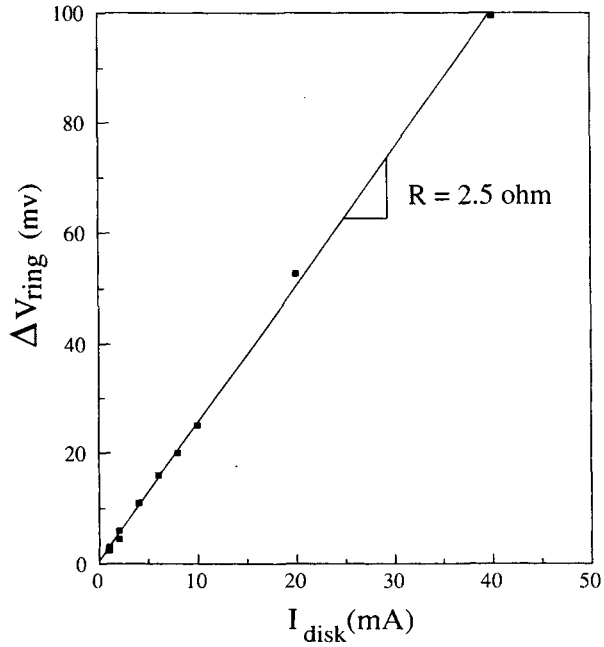

Figure 15. Change in the ring potential as measured by the current-interrupt, 0.2 M $NiCl_2$, 1 M NaCl.

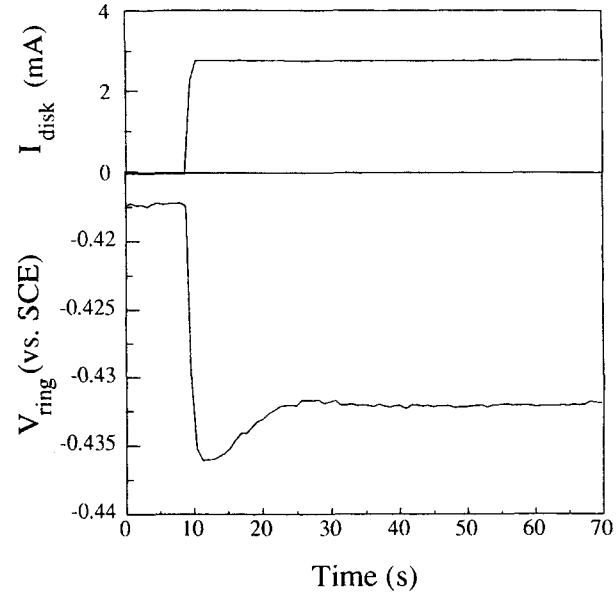

Figure 16. Nickel deposition onto a platinum disk electrode, 900 rpm, bulk pH = 2.95.

and the reference electrode is 2.5 ohms. This can be compared to the calculated ohmic resistance of 2.9 ohms based on this RRDE geometry and the electrolyte conductivity of 0.12 Ω^{-1} cm^{-1}.

Electrodeposition Experiments

In the Theory section, the relationship between the pH rise at the disk and the ring response was investigated. For the RRDE used in these experiments, geometry B, cathodic shifts larger than 12 mV are needed for a surface pH rise larger than 2 units (see Figure 10). In the presence of species such as MOH^+ ions or other proton-donor buffering agents, the transition to large pH rise occurs at even larger cathodic shifts.

Nickel electrodeposition

Current efficiency of nickel deposition is a measure of the division of total current into metal deposition and hydrogen evolution. The ring responds to the hydrogen evolution that takes place along with nickel deposition at the disk electrode. An example of one such measurement is shown in Figure 16 which is obtained by stepping the current on the initially bare platinum disk to 6 mA/cm^2. It should be remembered that platinum is a better catalyst for hydrogen discharge than is nickel. Initially, the partial current of hydrogen is high on the bare platinum, leading to a large cathodic shift in the ring potential. As the disk becomes covered with nickel, the hydrogen partial current is reduced as reflected in the ring potential moving in the positive direction (that is, smaller pH rise at the disk surface).

The change in the ring potential as a function of the total disk current is compared for hydrogen evolution by itself and during co-discharge with nickel in Figure 17. Nickel was electroplated from a 0.2 M solution of $NiCl_2$ Certified Fisher Scientific with a bulk pH of 2.9 and 1 M NaCl as supporting electrolyte. If the cathodic shift of the ring potential, in its

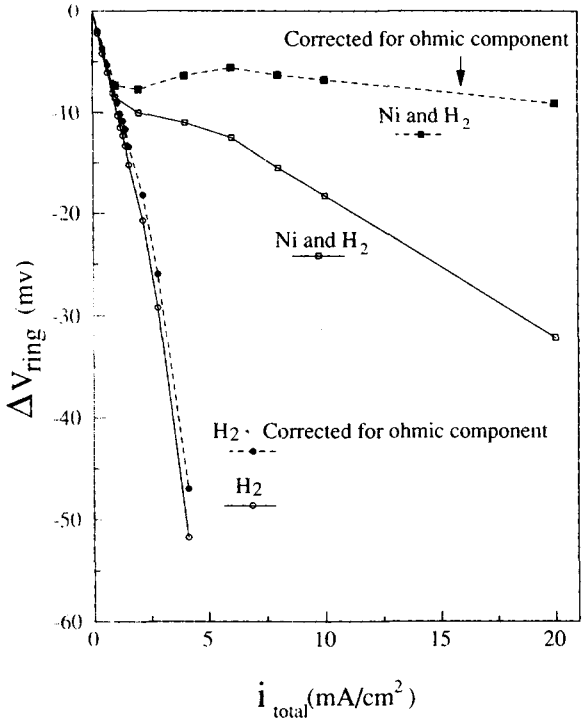

Figure 17. Ring response to hydrogen evolution by itself, and to nickel deposition with simultaneous hydrogen evolution, bulk pH = 2.90, 0.2 M $NiCl_2$, 900 rpm.

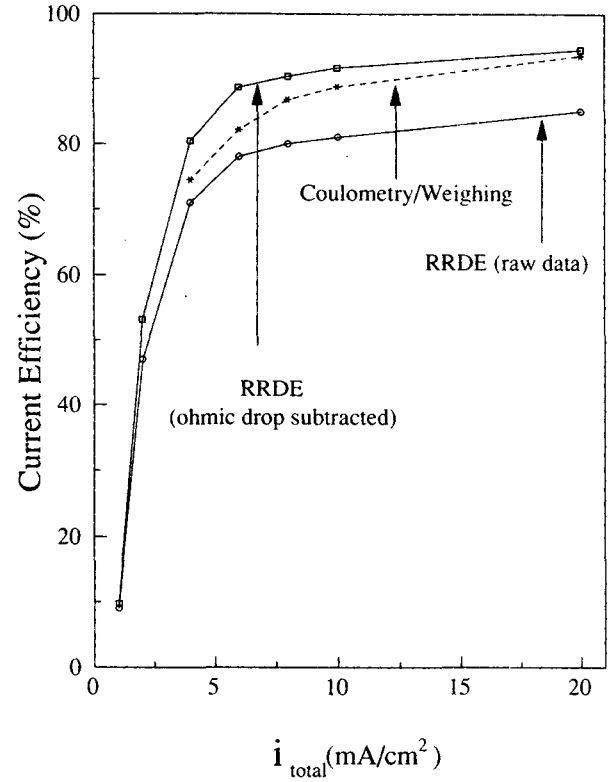

Figure 18. Current efficiency of nickel deposition as measured with the rotating ring-disk electrode and by weighing the deposit, bulk pH = 2.90, 0.2 M $NiCl_2$, 900 rpm.

entirety, is caused by hydrogen evolution, the partial current of hydrogen during nickel deposition can be easily evaluated from measurements in the absence of nickel ions. As discussed earlier, the ring response to hydrogen evolution is related to the fraction of mass-transfer limited current. Since the ionic strength of the nickel plating solution was adjusted to be close to the hydrogen evolution calibration baths, the difference in diffusivities and viscosities should be insignificant; this leads to the same limiting hydrogen current for a given bulk pH and agitation speed.

Several experiments using replaceable copper disk electrodes were conducted to determine the current efficiency of nickel electrodeposition independent of the RRDE method. The total charge passed during deposition was monitored with the built-in coulometer of the PAR 273 potentiostat. A Mettler Instrument Corp. analytical balance with a sensitivity of 0.1 mg was used to weigh the electrodes before and after electrodeposition. The charge going into nickel plating is inferred from the added weight of the electrode and Faraday's law. The current efficient results, $\eta = 1 - [i_{H_2}/i_{tot}]$, as estimated by both methods are shown in Figure 18. The values obtained by the RRDE method are less than the coulometry/weighing results. This can be attributed to the ohmic component of the ring potential which must be corrected. As discussed previously, the ohmic component is proportional to the total current which can be significant at high currents associated with the metal deposition. The ring response without the ohmic component is shown in Figure 17 for hydrogen evolution by itself and concurrent with nickel electrodeposition. Using the corrected values of the ring response, the current efficiency obtained from the RRDE measurements increases, shown in Figure 18, and the agreement between the RRDE and the coulometry/weighing methods improves. Note that the weighing/coulometry results are biased towards smaller values by possible deposit peel-off, and a reduction of current density by roughening of the surface after long deposition times. The RRDE method is biased toward larger values since the presence of nickel-hydroxide ions can buffer the ring response, as discussed earlier.

The ring response to the electrodeposition of nickel with concurrent hydrogen evolution, corrected for the ohmic drop, can be used to assess the interfacial pH at the disk. A typical set of such results was shown in Figure 17. Comparison of the ring response, corrected for the ohmic drop, to Figure 10 indicates that the pH at the disk surface has risen by 1 unit. The flattening of the ring potential-shift, as a function of the total disk current, means that the hydrogen current is not changing, and it is the nickel current which is increasing with current density. The small rise in pH during nickel deposition under the conditions of this study are in good qualitative agreement with the findings of Deligianni and Romankiw (1990) who used a glass pH electrode behind a rotating mesh cathode. They also observed that in the presence of metal ions hydrogen evolution leads to a much smaller interfacial pH rise.

Iron electrodeposition

Application of the RRDE method for deposition of iron from a solution containing ferrous ions was investigated. Fig-

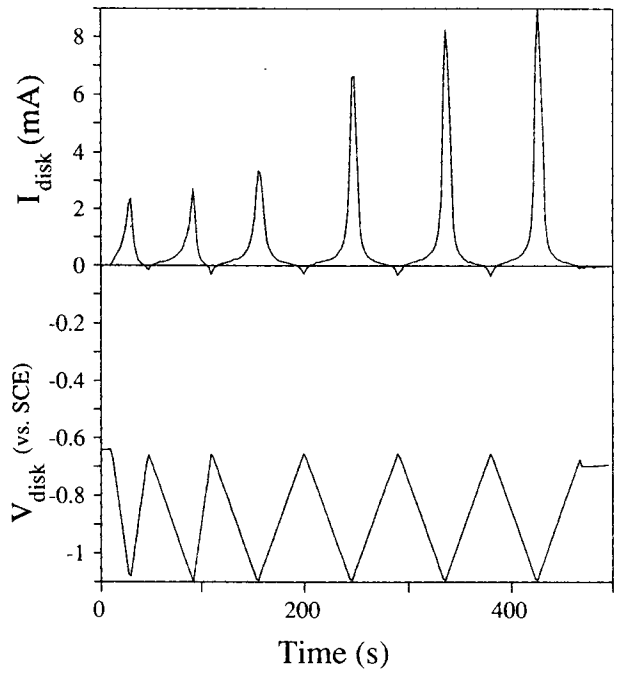

Figure 19. Iron deposition onto an initially bare platinum disk from 0.04 M $FeSO_4$ at 900 rpm, 25 mV/s, and 10 mV/s.

ure 19 shows the disk current as a function of a cathodic potential sweep for a solution of 0.04 M $FeSO_4$, 1 M NaCl with a bulk pH of 3. The current on the initially bare platinum disk electrode increases in each sweep cycle. The ring response when corrected for the ohmic drop, Figure 20, shows a periodic behavior indicating the partial current of hydrogen is not

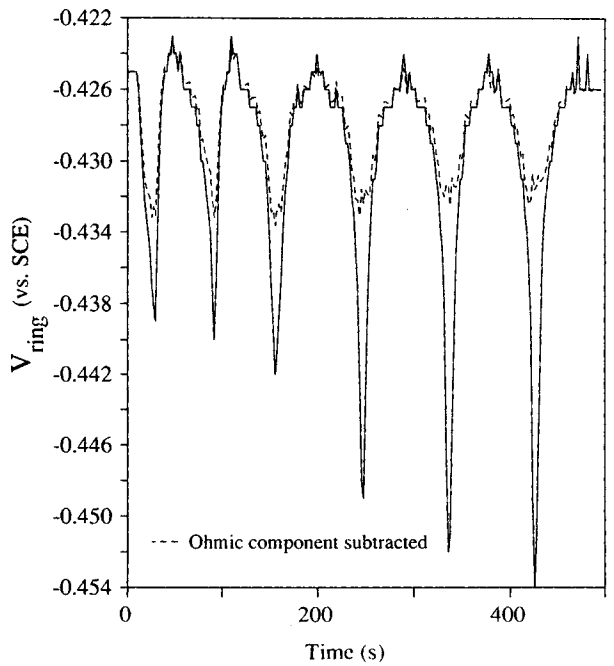

Figure 20. Measured ring response during iron deposition.

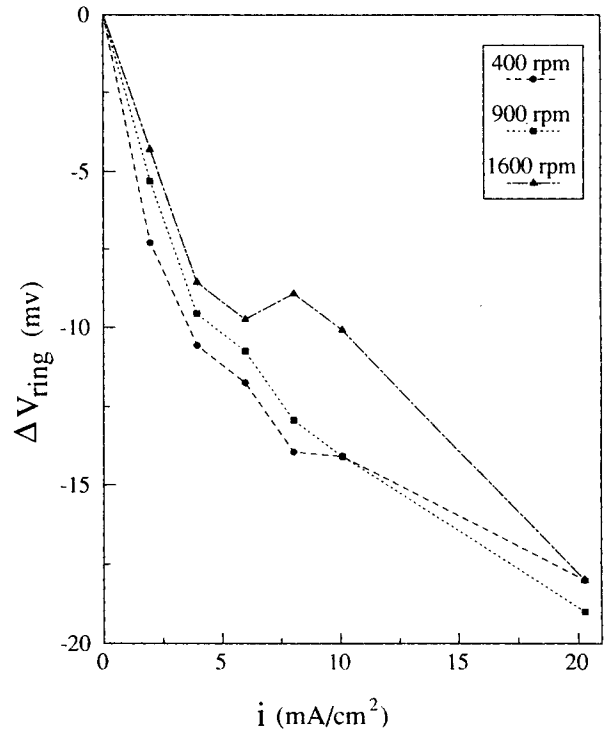

Figure 21. Nickel-ring deposition at various rotation speeds, 0.2 M nickelous, 0.005 M ferrous, 0.4 M boric acid, 1 M NaCl, pH = 3.1.

changing from cycle to cycle. The implication is that the increase in the disk current is caused by the increasing partial current of iron as the platinum disk becomes covered with electrodeposited iron. The maximum ring potential shift is -10 mV which is less than 1 pH unit rise on the disk surface.

Nickel-iron electrodeposition

Nickel-iron alloys were deposited from a solution of 0.2 M $NiCl_2$, 0.005 M $FeSO_4$, 1 M NaCl, and 0.4 M boric acid. The concentration of the metal ions and the range of current densities and agitation rates were the same as the study by Andricacos et al. (1989). For different agitation speeds, nickel-iron was plated onto the disk electrode while the ring potential was monitored at open-circuit. The steady-state potential shift of the ring, corrected for ohmic drop, for agitation speeds of 400, 900 and 1,600 rpm is shown in Figure 21. At higher current densities, the hydrogen current and surface pH increase which correspond to a larger shift in the ring potential. The ring response is also more cathodic at lower agitation rates indicative of a higher pH rise at the disk. The shift in the ring potential translates to different values of the pH rise depending on the value of the dissociation constant for $NiOH^+$ and $FeOH^+$, as shown in Figure 22. At current densities below 8 mA/cm^2, the interfacial pH rise for all agitation speeds, and different K_d values, is less than 1 unit. At higher current densities, the pH rise is about 3 units for a large dissociation constant of $K_d = 10^{-5}$ and only 1 unit for $K_d = 2.5 \times 10^{-8}$.

The composition of Ni-Fe alloys electrodeposited under similar conditions by Andricacos et al. show that the percentage

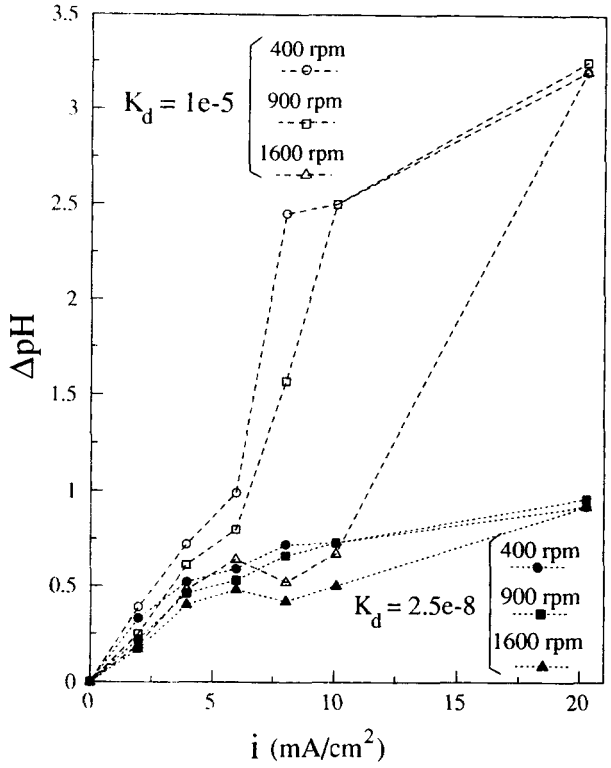

Figure 22. Interfacial pH rise at the disk during Ni-Fe electrodeposition corresponding to the data in Figure 21.

of iron in the alloy increases rapidly with current density, and passes its maximum of 40 weight percent at current densities less than 10 mA/cm^2. In this range of current density, our measurements indicate that the pH at the interface is only about 4. Even at higher currents, the interfacial pH is at most 6. The minimum pH for precipitation of a solid metal-hydroxide with the concentration of metal ions in this electrolyte is 6.6 for nickel and 7.8 for ferrous hydroxide (Pourbaix). This is strong evidence that the inhibition of nickel deposition during nickel-iron plating can occur with only a small interfacial pH rise. Our simulation of nickel-iron alloy deposition based on a mechanism involving $NiOH^+$ and $FeOH^+$ ions predicts a pH rise of less than 1 unit at the disk surface, in qualitative agreement with the RRDE measurements.

Conclusions

Potentiometric application of a pH sensitive ring electrode for *in-situ* determination of pH at a rotating disk electrode has been analyzed. The two-dimensional transport of protons in the RRDE system including homogeneous reactions was investigated. Equal-diffusivities were assumed to allow linearization of the transport equations leading to analytical solutions. It is shown that at a given hydrogen current, the ring response depends on the RRDE geometry, bulk pH, fraction of the hydrogen limiting current, concentration of metal ions and dissociation constant of metal-hydroxide complexes, degree of supersaturation of dissolved hydrogen, and solution conductivity.

A platinized ring electrode in a hydrogen-saturated electrolyte has been shown to be a stable and reproducible sensor for the pH at a rotating disk. This method was used to measure the interfacial pH rise during the electrodeposition of nickel, iron, and nickel-iron which involve simultaneous hydrogen evolution. Effects of agitation, current density and substrate coverage on the ring potential were investigated. For the conditions of this study, the rise in interfacial pH was found to be less than 1 unit for pure nickel and iron, and from 1 to 3 units for nickel-iron alloy depending on the dissociation constant of the metal-hydroxide ion complexes. These results indicate that the "anomalous codeposition" of nickel-iron can take place without a high surface pH and formation of any metal hydroxide precipitate.

This mode of operating the RRDE can also be applied to measure current efficiency in a fast, nonintrusive and *in-situ* manner. Alternate methods such as weighing are laborious and require long deposition times to obtain sufficient amounts of deposit. Roughening of the surface, hence changing the true current density, and even a loss of deposit by peel-off are common sources of errors. The RRDE method is immune to these problems and can be advantageously used in developing plating baths and optimizing process parameters.

Notation

a = rotating disk hydrodynamic constant, 0.51023
C = concentration, mol/cm^3
D = diffusion coefficient, cm^2/s
f = fugacity, atm
F = Faraday's constant, 96487 Cb/eq
H = Henry's law constant
i = current density, A/cm^2
$i_{H^+,lim}$ = hydrogen ion limiting current in the absence of MOH^+ ions
I = fraction of the limiting current
I_{disk}, I_{tot} = current, A
I_{LM} = enhancement of the limiting current by metal-hydroxide ions
k_s = salting-out parameter, M^{-1}
K_d = dissociation constant of MOH^+ ions
K_w = water dissociation constant
r = radial distance, cm
R = universal gas constant, 8.3143 J/mol·deg
R_{rd} = ohmic resistance between the ring and the disk
S = solubility, M
T = absolute Temperature, K
x = mole fraction
y = axial distance, cm

Greek letters

Φ = electric potential, V
κ = conductivity, mho/cm
Ω = disk rotation speed, radian/s
ν = kinematic viscosity, cm^2/s
Θ = dimensionless concentration, $\Theta = (C - C^d)/(C^b - C^d)$
ζ = dimensionless axial distance, defined after Eq. 2

Superscripts

b = bulk
d = disk surface

Subscripts

lim = mass-transfer limiting
tot = total

Literature Cited

Albery, W. J., and S. Bruckenstein, "Ring-Disk Electrodes: 2. The-

oretical and Experimental Collection Efficiencies," *J. Chem. Soc., Farad. Trans. 1*, **79**, 1920 (1965).
Albery, W. J., and E. J. Calvo, "Ring-Disc Electrodes: 21. pH Measurement with the Ring," *J. Chem. Soc., Farad. Trans. 1*, **79**, 2583 (1983).
Albery, W. J., and A. R. Mount, "Ring-Disc Electrodes: 22. Theory of the Measurement of Proton Fluxes at the Disc," *J. Chem. Soc., Farad. Trans. 1*, **85**(5), 1181 (1989).
Albery, W. J., and A. R. Mount, "Ring-Disc Electrodes: 23. Studies of Proton Fluxes at a Thionine-coated Electrode," *J. Chem. Soc., Farad. Trans. 1*, **85**(5), 1189 (1989).
Andricacos, P. C., C. Arana, J. Tabib, J. Dukovic, and L. T. Romankiw, "Electrodeposition of Nickel-Iron Alloys: I. Effect of Agitation," *J. of Electrochem. Soc.*, **135**, 1172 (1989).
Bek, R. Yu, and L. I. Borodikhina, "Calculation of the pH in the Layer Next to the Cathode During Hydrogen Evolution from Buffer Solutions," *Sov. Electrochem.*, 121 (1978).
Dahms, H., and I. M. Croll, "The Anomalous Codeposition of Iron-Nickel Alloys," *J. of Electrochem. Soc.*, **112**, 771 (1965).
Deligianni, H. and L. R. Romankiw, "A Rotating pH Electrode for Measurement of Surface pH During Electrolysis; Study of NiFe Electrodeposition," Extended Abstracts, **90-2**, Electrochemical Society (1990).
Dukovic, J. O., and C. W. Tobias, "The Influence of Attached Bubbles on Potential Drop and Current Distribution at Gas-Evolving Electrodes," *J. of Electrochem. Soc.*, **134**, 331 (1987).
Gunther, H., R. Wetzel, and R. Muller, "A New Method for pH Measurement in the Immediate Vicinity of the Electrode Surface," *Electrochimica Acta*, **24**, 237 (1979).
Hessami, S., and C. W. Tobias, "A Mathematical Model for Anomalous Codeposition of Nickel-Iron on a Rotating Disk Electrode," *J. of Electrochem. Soc.*, **136**, 3611 (1989).
Hildebrand, F. B., *Advanced Calculus for Applications*, 2nd ed., Prentice-Hall, Englewood Cliffs, NJ (1976).
Hills, C. J., and D. J. G. Ives, "The Hydrogen Electrode," *Reference Electrodes: Theory and Practice*, D. J. Ives and G. J. Janz, eds., Academic Press, New York (1961).
Kuhn, A. T., and C. Y. Chan, "pH Changes at Near-Electrode Surfaces," *J. of Applied Electrochem.*, **13**, 189 (1983).
Levich, V. G., *Physiochemical Hydrodynamics*, Prentice-Hall (1962).
Matulis, J., and R. Slizys, "On Some Characteristics of Cathodic Processes in Nickel Electrodeposition," *Electrochimica Acta*, **9**, 1177 (1964).
Newman, J., "Resistance for Flow of Current to a Disk," *J. of Electrochem. Soc.*, **113**, 501 (1966).
Newman, J., "Ohmic Potential Measured by Interrupter Techniques," *J. of Electrochem. Soc.*, **117**, 507 (1970).
Newman, J., and W. H. Smyrl, "Ring-Disk and Sectioned Disk Electrodes," *J. of Electrochem. Soc.*, **119**, 212 (1972).
Newman, J., *Electrochemical Systems*, Prentice Hall, Englewood Cliffs, NJ (1973).
Newman, J., and J. J. Miksis, "Primary Resistances for Ring-Disk Electrodes," *J. of Electrochem. Soc.*, **123**, 1030 (1976).
Perry, R. H., and C. H. Chilton, *Chemical Engineers' Handbook*, 5th ed., McGraw-Hill Book Company (1973).
Pourbaix, M., *Atlas of Electrochemical Equilibria in Aqueous Solutions*, Nat. Assoc. of Corrosion Engrs. (1974).
Prausnitz, J. M., R. N. Lichtenthaler, and E. M. de Azevedo, *Molecular Thermodynamics of Fluid-Phase Equilibria*, p. 377, 2nd edition, Prentice-Hall, Englewood Cliffs, NJ (1986).
Press, W. H., B. P. Flannery, S. A. Teukolsky, and W. T. Vetterling, *Numerical Recipes*, Cambridge Univ. Press (1986).
Romankiw, L. T., "pH Changes at the Cathode During Electrolysis of Ni, Fe, Cu and Their Alloys and a Simple Technique for Measuring pH Changes at Electrodes," *Electrochemical Society Proceeding Volume*, **87-17**, 301 (1987).
Ruetschi, P., and R. F. Amile, "Solubility of Hydrogen in Potassium Hydroxide and Sulfuric Acid. Salting-out and Hydration," *J. of Phys. Chem.*, **70**, 718 (1966).
Shibata, S., "The Anodic Behavior of Cathodically Prepolarized Bright Platinum Electrode in Sulfuric Acid Solution," *The Chem. Soc. of Japan*, **33**, 1635 (1960).
Sillen, L. G., *Quart. Rev.*, XIII, 146 (1959).

Manuscript received Dec. 19, 1990, and revision received July 2, 1992.